Ductile crack initiation and growth on a plasticized Polyvinylchloride during air bag deployment

Lucien Laiarinandrasana, C. Bertaux, N. Amouroux, C. Ovale Rodas

Noname manuscript No.
(will be inserted by the editor)

Ductile crack initiation and growth on a plasticized Polyvinylchloride during air bag deployment

L. Laiarinandrasana · C. Bertaux · N. Amouroux · C. Ovalle Rodas

Received: date / Accepted: date

Abstract With the goal of ensuring the security of passengers for automotive industry, the present work addresses the ductile fracture process of plasticized PVC. Dedicated clamped single edge notch bending (SENB) specimens were used to characterize the mechanisms of crack initiation and propagation for the studied material. The exploitation of the experimental database associated with finite element simulation of the crack propagation allowed, on the one hand, the calibration factor η_{p} of this specific SENB specimen to be established, as a function of the crack depth ratio. On the other hand, the fracture toughness of the studied plasticized PVC was estimated to be 10.8 kJ/m^2, value which was close to that reported in the literature for modified PVC. By using this fracture toughness value, a methodology aiming at the prediction of ductile crack initiation of the PVC skin integrated into a real dashboard (full scale test) was proposed.

Keywords Fracture mechanics · Impact strength · Polymers · Ductile failure · Finite Elements

L. Laiarinandrasana
MINES ParisTech, PSL University, MAT - Centre des Matériaux, CNRS UMR 7633,
BP 87 91003 Evry, France
E-mail: lucien.laiarinandrasana@mines-paristech.fr

C. Bertaux
MINES ParisTech, PSL University, MAT - Centre des Matériaux, CNRS UMR 7633,
BP 87 91003 Evry, France
E-mail: clement.bertaux@mines-paristech.fr

N. Amouroux
Westlake Couponds Holding 1bis rue Maurice Hollande
51100 Reims, France
E-mail: nicolas.amouroux@westlake.com

C. Ovalle Rodas
MINES ParisTech, PSL University, MAT - Centre des Matériaux, CNRS UMR 7633,
BP 87 91003 Evry, France
E-mail: cristian.ovalle_rodas@mines-paristech.fr

1 Introduction

The correct deployment of airbag spreading is a major concern for the security of passengers in the automotive industry. The design and elaboration of the dashboard is one of the key features for obtaining the required specifications. Plasticized PVC skins are commonly used for the top surface of the three layers of the dashboard.

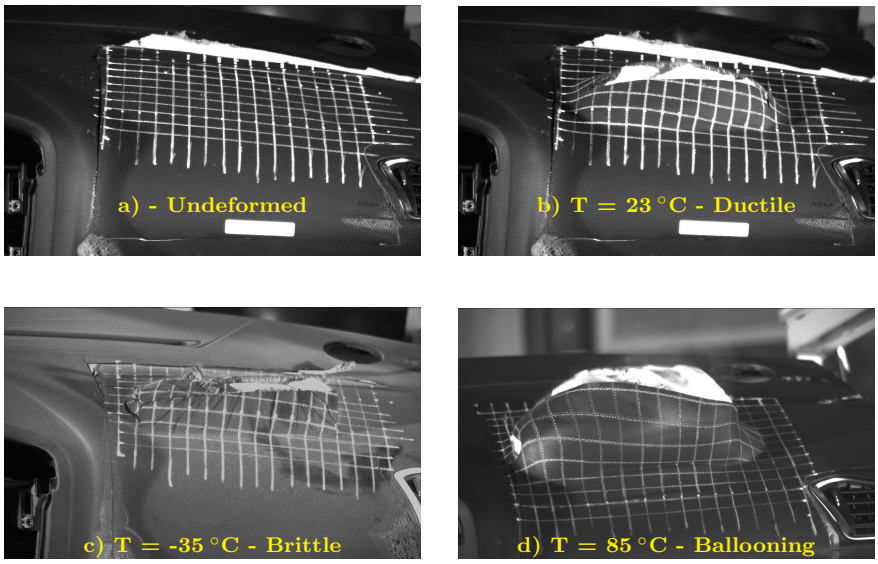

Fig. 1 Tests at full scale of an air-bag deployment: a) Undeformed state of the airbag window; b) correct ductile tearing at 23 °C; c) brittle failure at -35 °C where secondary transverse cracks can be observed; d) ballooning effect at 85 °C inducing delay or non opening.

To assess the role of the system in the spreading of the airbag, full scale tests have been carried out at various temperatures. Figure 1 illustrates some salient results of these tests which allow a better analysis of the deformation and failure of the opening of windows on the airbag box during deployment.The grid cell size was about 10 mm in the initial undeformed state (fig. 1a). From these tests, it was observed that:

- At 23 °C (fig. 1b), a net ductile tearing of the skin, following the scoring direction and accompanied by the deformation of the top surface of the airbag box, was observed. This is the desired fracture process. Using Digital Image Correlation (DIC) software, the impact speed applied to the PVC skin was estimated to be around 25 m/s;
- At -35 °C (fig. 1c), but at the same impact speed, a brittle failure of the skin occurred with small deformations. The main crack was on the surface plane and followed the direction of the inner score already made on the

plasticized PVC outer skin. The presence of secondary transverse cracks could be noticed. These may provoke fragmentation [1] of the dashboard, accompanied by the projection of the pieces of the material and so would be dangerous for the passengers;
– At 85 °C (fig. 1d), at the same impact speed, a significant deformation of the box together with an extreme extension of the skin delayed the opening time, if it occurred, as ballooning could prevent the opening of the box. This situation is the most dangerous condition which needs to be avoided even though the ultimate failure could also be qualified as ductile.

Full scale experiments, as reported above, are very costly. Therefore, a research programme was elaborated to directly test the plasticized PVC skin [2]. One grade of plasticized PVC was selected, the most common one used in the automotive industry.PVC skin plates were provided by the Westlake Global Compound company. Scoring was added as a pre-crack on the samples using a robot for better reproducibility. The desired ratio between the score depth and the total thickness was about 0.5.

Standardized Charpy tests [3,4] are commonly recommended to characterize the failure of plastics by impact. They enable the determination of the impact strength of the material by utilizing notched specimen with precise notch root radius. In the present work, the robot cut induced more acute crack with a notch root radius tending to zero. Moreover, the knowledge of the impact strengths allows the classification of plastics regarding their brittle fracture behaviour. As the desired failure mode is the ductile one for the plasticized PVC under study, this constitutes a limitation for the use of Charpy tests. Indeed, for very ductile plastics, the specimen may not fail after the impact. In this extreme case of no failure, the impact strength cannot be determined. Additionally, as mentioned above (test at 85 °C), this is the most dangerous situation. The aim of this work is then to characterize the ductile failure of the plasticized PVC, by using the fracture mechanics tools.

To achieve this goal, the present paper starts by recalling previous results [2] where the domain of interest, in terms of temperatures and impact speeds that emphasizes the ductile failure of the material, has been determined. Then, the methods used are described in the second section. The design of an experimental setup adapted to the material so as to obtain ductile failure characteristics is developed. The load parameters and the failure criteria for ductile fracture of polymers proposed by fracture mechanics theory [5,6] are introduced. The Finite Element analysis allowing the computation of the load parameters for complex cracked geometries is described at this stage. The section listing the results follows, starting from the specific mechanisms of crack initiation and growth, proper for the studied plasticized PVC. The fracture toughness of the material was determined by taking these mechanisms into account. The relationship between the obtained fracture toughness and the impact strength is then established. The last part of the paper consists of a set of discussions that propose a methodology to predict the ductile crack initi-

ation on the PVC skin integrated into the dashboards thanks to the knowledge of the fracture toughness of the material.

2 Background

Impact tests were carried out using an Instron CEAST 9350 drop tower impact system [7]. The samples, consisting of thin and soft plates, had to be gripped along a circular section. Details of the CEAST 9350 machine have been described elsewhere [2]. About one hundred test results have been analysed, corresponding to 3 tests for each selected test temperature: (-6, -3, 0, 5, 10, 15, 20, 25°C) and each selected impact speed: (2, 4.4, 6, 10 m/s).

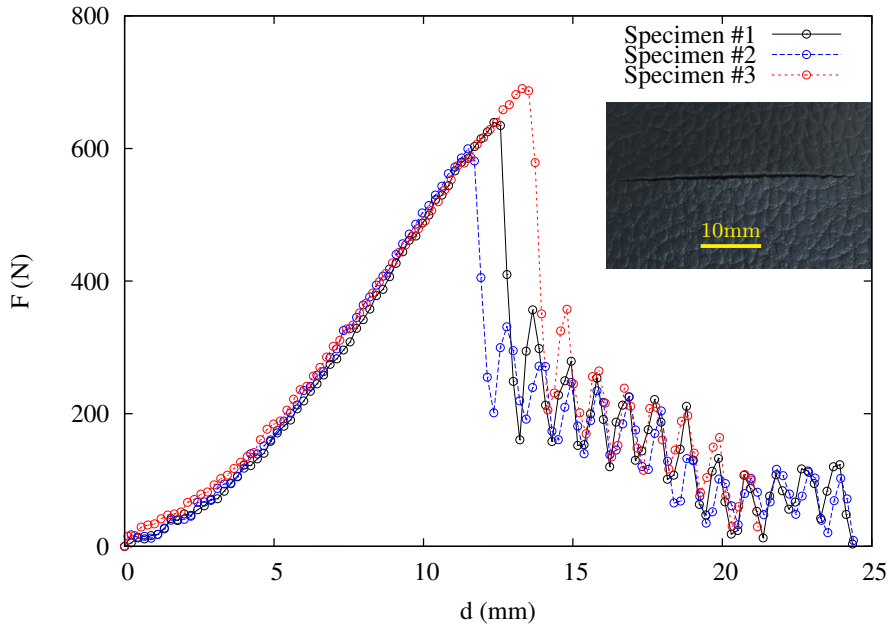

Fig. 2 Load (F) *versus* deflection (d) curves for scored thin plates tested at 4.4 m/s and 20 °C. Ductile fracture surface at the macroscopic scale is shown.

The load *versus* deflection curves for the three tests at 20° C and at an impact speed of 4.4 m/s are shown in fig. 2. A first loading stage was observed up to a load of about 650 N. Then, a first load drop appeared followed by a gradual decrease with apparent oscillations. The slope of the first drop appeared to be same for the three tests. Additionally, the fracture surfaces of the tested samples exhibited characteristics of ductile failure.

From the load *versus* deflection curves, four main characteristic mechanical parameters were deduced:

– the stiffness of the system that corresponded to the slope of the linear part of the curve: $\frac{\Delta F}{\Delta d}$ where F is the load and d is the deflection;
– the deflection and the load at failure, respectively d_F and F_F, related to the last point before the abrupt drop of the load, *i.e.* at the onset of failure;
– the fracture energy A_F determined by integration of the area under the load *versus* deflection curve up to (d_F, F_F):

$$A_F = \sum_{i=1}^{F} \frac{(F_i + F_{i-1})}{2}(d_i - d_{i-1}) \quad (1)$$

The so-called impact strength here consisted in relating the fracture energy in eq. (1) to the fracture surface area $\Phi(t - a)$ where Φ is the diameter of the hemispherical impactor, 't' is the thickness of the skin, and 'a' is the crack depth. In fact, this operation consisted of integrating the area under the net stress *versus* the deflection curve; the net stress being the ratio of the load per unit of the fractured surface.

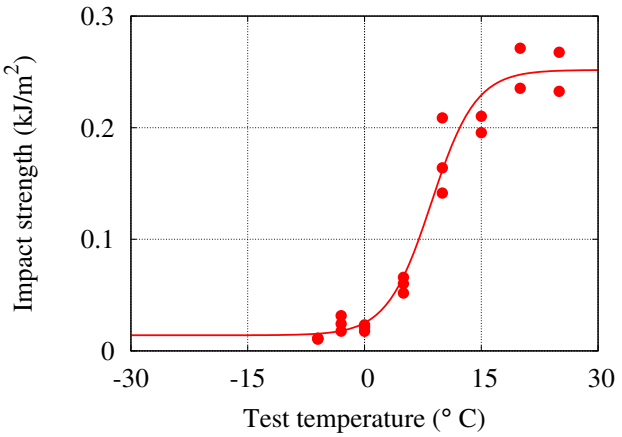

Fig. 3 Evolution of the impact strength with respect to the test temperature.

The evolution of the impact strength of the studied plasticized PVC for the impact speed of 4.4 m/s as a function of the test temperature is shown in figure 3. Attention should be paid here to the upper shelf corresponding to the ductile mechanisms of failure. Typically, it could be concluded that, under these test conditions, the impact strength of the plasticized PVC was about 0.25 kJ/m^2.

The extension of this result to the other impact speeds was assessed by determining how the Ductile Failure Threshold Temperature (T_{dth}) evolved with respect to the impact speed as illustrated in fig. 4. Although the impact speed of 25 m/s was not reached in this study, this plot indicated that T_{dth}

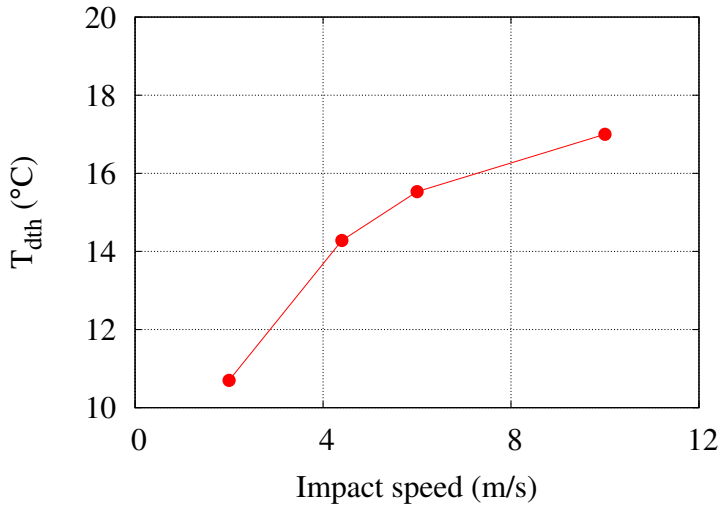

Fig. 4 The temperature to ductile fracture threshold (T_{dth}) as a function of the impact speed.

tended to stabilise and would be lower than 20° C. This has been confirmed by the ductile failure obtained for the full scale test at 23° C shown in fig. 1b.

Theoretically, the impact strength value of 0.25 kJ/m^2 determined on the upper shelf is not dependent on the impact speed. On the other hand, for pre-cracked specimens, the relationship between the impact strength and the fracture toughness has been investigated in several research papers on metals [8]. The present work aims at the determination of the fracture toughness of the plasticized PVC under study by using the fracture mechanics approach.

3 Methods

3.1 Experiments

PVC skin plates of 90 mm × 90 mm size and with 1.2 mm ± 0.1 mm thickness were provided by the Westlake Global Compound company. Scoring was added as a pre-crack on the plates using a robot for better reproducibility. The desired ratio between the score depth and the total thickness was about 0.5. The robot cut the material so as to keep a retentive ligament thickness of 0.6 mm. This implied an uncertainty on the crack depth ratio due to the real thickness of the skin and the roughness of the pattern on its top surface.

Rectangular specimens were then machined from the scored thin plates, using a punch especially assembled for better dimension reproducibility. The main dimensions of these rectangular scored samples were 90 mm in length and 29.8 mm in width. They mimic the fracture mechanics Single Edge Notch

Bending (SENB) specimens for rigid plastics. The initial contact between the impactor and the sample constituted the major difference from the above mentioned CEAST test and the present experiments: a point and a line, respectively for the hemispherical impactor of CEAST and for the present SENB-like specimen.

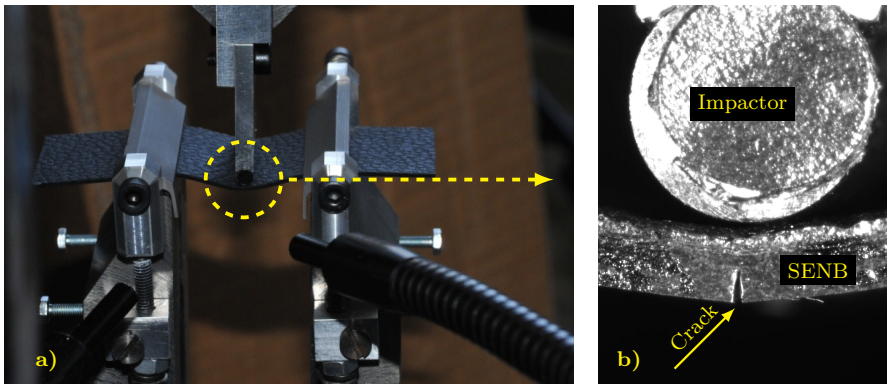

Fig. 5 Experimental setup for clamped Single Edge Notch Bending (SENB) test: a) Top view where the patterns on the top skin of plasticized PVC plate can be observed; b) Details of the non deformed crack tip

To better understand the mechanisms of ductile crack initiation and propagation near the impacted zone of the scored thin sample, SENB specimens were tested using an Instron 5982 (up to 100 kN force capacity), with an additional and adapted load cell of 1 kN. Figure 5a illustrates the top view of the experimental setup where span "S" of the rollers was fixed at 30 mm. Moreover, the impactor pin and the rollers had the same root radius of 2 mm. The plasticized PVC being extremely soft/flexible, unlike the classical SENB setup, specific jaws were designed to prevent any sample displacement during the test. It should be mentioned that the same boundary conditions were applied for the impact tests of pre-cracked thin plate. The data collected during the test consisted of the load and the corresponding deflection.

Figure 5b details the region near the crack tip in the undeformed state. A video camera was placed in front of one of the side surfaces so as to synchronize the load and the deflection recorded with the crack opening displacement and the advance of the crack. Due to the large strain experienced by the material, the camera had to be motorized to follow the position of the sample. The test's deflection speed, of about 6 mm/s, was selected to match that of the motor.

3.2 Load parameters - Failure criteria

Fracture mechanics approach uses the concept of load parameter and failure criterion. The load parameter is the relevant variable combining the applied load and the characteristic lengths of the crack and the cracked body. The failure criterion consists of the critical value of the aforementioned variable [5, 6,9–11].

This work focuses on two load parameters: a kind of fractured surface energy density, noted as Γ corresponding to the area under the load *versus* deflection curve (eq. (1)), related to the area of the remaining ligament; and the J-integral recommended by the non linear fracture mechanics. The two corresponding failure criteria are the impact strength (Γ_c) [8,12] and the fracture toughness (J_c), respectively.

3.2.1 Fractured surface energy density (Γ)

This parameter coming from the load and the deflection that have been measured during the test can be written as:

$$\Gamma = \frac{A(F, d)}{B(W - a)} \tag{2}$$

with:

- $A(F, d)$ the area under the load *versus* deflection curve;
- B the thickness of the specimen[1];

[1] In the present study, in line with the commonly used terminology of the fracture mechanics, the thickness B and the width W of the specimen, in eqs. 2 and 3, correspond respectively to the width and the thickness of the machined rectangular specimens.

– W the Width of the specimen;
– a the crack depth.

For dedicated Charpy notched specimen, the critical surface energy density at failure (maximum load) corresponds to the impact strength of the material. Here, although a sharp crack is considered, Γ_c will be considered as the impact strength. The evolution of the Γ parameter with respect to the deflection should be analyzed so as to better understand the limits of this key parameter for an engineering approach.

3.2.2 J-integral (J)

In fact, for pre-cracked specimens, the curve to be analysed should be the load *versus* the crack opening displacement (COD). This latter variable is more local than the deflection. However, its measurement was not as easy: it came from video acquisition. The area under this curve is known to be related to the J-integral, the load parameter recommended in non-linear fracture mechanics analysis [5,6].

$$J_t = \eta_e \frac{A_e(F, COD)}{B(W - a)} + \eta_p \frac{A_p(F, COD)}{B(W - a)} \tag{3}$$

with:

– B the thickness of the specimen;
– W the Width of the specimen;
– a the crack depth;
– η_e and η_p, respectively elastic and plastic calibration factors dependent on the crack depth ratio, the geometry of the specimen and the type of test. According to Williams [5], this factor is assumed to be constant and equal to 2 for classical SENB geometry. For the present clamped SENB specimen, these factors are unknown;
– $A_e(F, COD)$ and $A_p(F, COD)$, respectively the elastic and plastic areas under the load-crack opening displacement curve. The partition between these areas can be obtained once the linear correction of the load *versus* COD curve [6] had been operated.

For the sake of simplicity, many studies for polymer materials utilized only the plastic part of the J-integral [5].

$$J_p = \eta_p \frac{A_t(F, COD)}{B(W - a)} \tag{4}$$

where $A_t(F, COD)$ is now the total energy corresponding to the total area under the load-crack opening displacement curve.

The critical value (at the maximum load) is defined as the fracture toughness of the material [13,14]. For impact speed, the fracture toughness is described by Mac Gillivray [15].

It is worth noting that equations (2) and (4) differ in the η_p factor and the relationship between the deflection and the notch opening displacement.

3.3 Finite Elements (FE)

Clamped SENB specimens tests were simulated using an in-house FE code: Z-set suite computing solution (http://zset-software.com/).

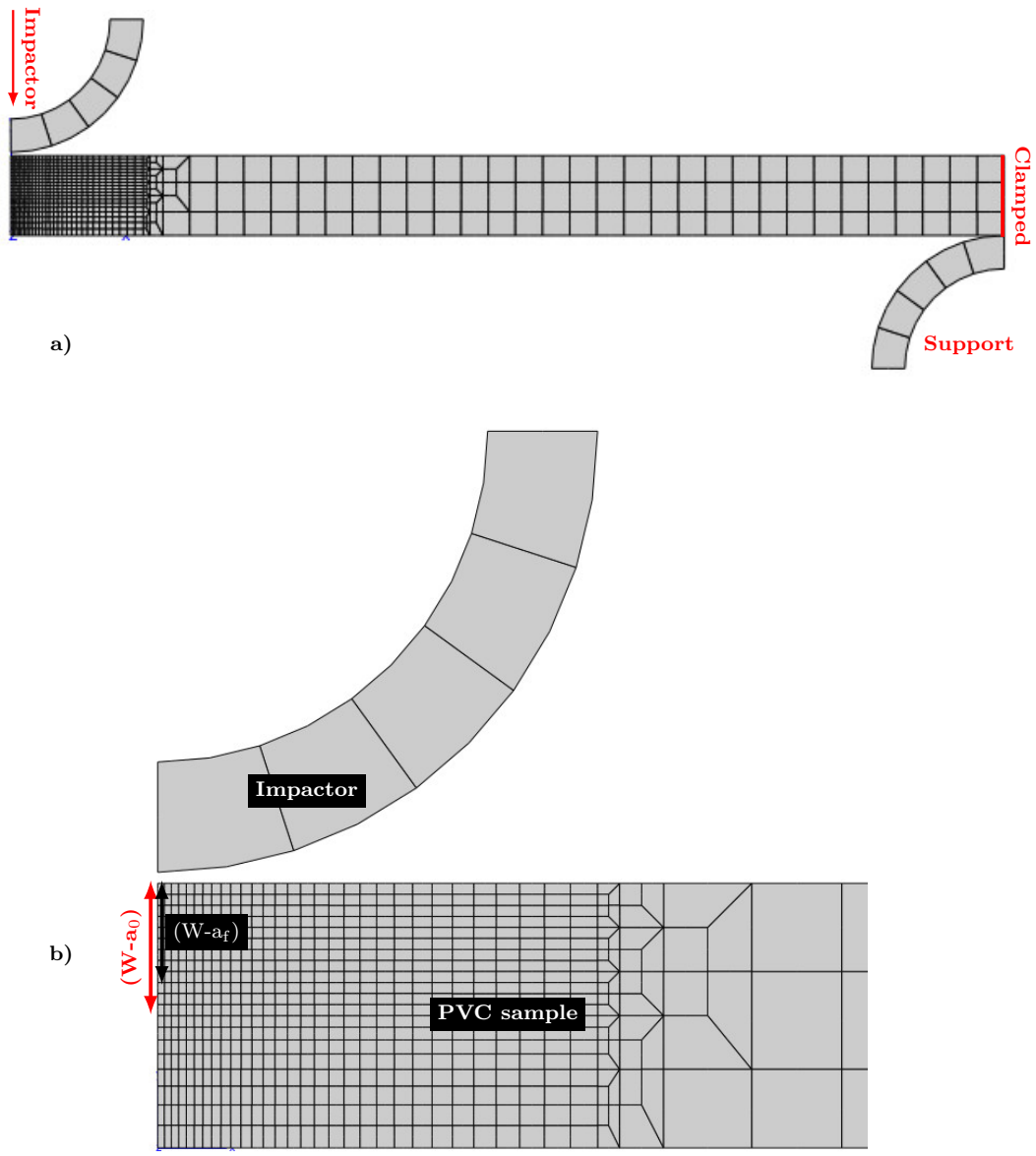

Fig. 6 Mesh of the clamped SENB specimen: a) Side view of the half specimen; b) Details of the crack tip region (refined meshes). *Note: Size of refined mesh = 50 μm so that* $a_0 - a_f =$ 150 μm *corresponds to the maximum crack extension before brittle failure.*

The FE computation used 2D iso-parametric plane strain elements with reduced integration. Only half of the specimen was meshed. Figure 6a illustrates the meshes for the PVC sample, the impactor and the roller. Near the crack tip, the meshes were refined (fig. 6b) so as to obtain an element side of 50 μm at the crack tip. The initial (W-a_0) and final (W-a_f) remaining ligaments are shown respectively by red and black arrows.

The loading was controlled by the displacement of the impactor during the test (deflection). The numerical approach used here did not intend to predict the failure of the specimen but dealt with a FE simulation of the crack propagation by imposing the history of the crack extension included in the experimental data from video camera acquisition. An attempt was then made to simulate the crack initiation and growth using the "release nodal degree of freedom" (`rndof`) technique [16,17]. This was done numerically by releasing gradually the nodes (in 6 steps for 3 quadratic elements) from the initial to the final remaining ligament, following the crack growth rate obtained experimentally.

The Z-set optimizer routine was first utilized to obtain a set of material coefficients using data from the load *versus* crack opening displacement curves. Then, the J-integral values with a propagating crack were computed using the de Lorenzi technique [18]. The comparison of these values with those of eq. (4) allowed the estimates of the η_p calibration factor to be achieved.

4 Results

The upper shelf impact strength was of key interest for engineering structures such as the skin of the dashboard. It was estimated to be 0.25 kJ/m^2 from macroscopic data: the load and the deflection. In this section, attention will be paid to the quasi-static tests (ductile fracture) carried out on clamped SENB specimens at room temperature T = 23°C and with an impact speed of 6 mm/s.

Figure 7 illustrates the side view of a deformed sample obtained from the video camera. The transverse cylindrical impactor moved down allowing the opening of the scored line. From this test, the load, the crack opening displacement (COD) and the crack extension (Δa) at the lateral surface were synchronized thanks to the embarked video–camera system. From this viewgraph, a large extension of the remaining ligament, leading to a crack tip opening displacement with an order of magnitude larger than the crack extension, was observed. At this deformed state, Δa and COD measurements were relative. They might be subjected to uncertainties.

4.1 SENB experimental data

The thinness and softness of the plasticized PVC material made it difficult to perform the tests. For reproducibility purposes, seven tests were carried out

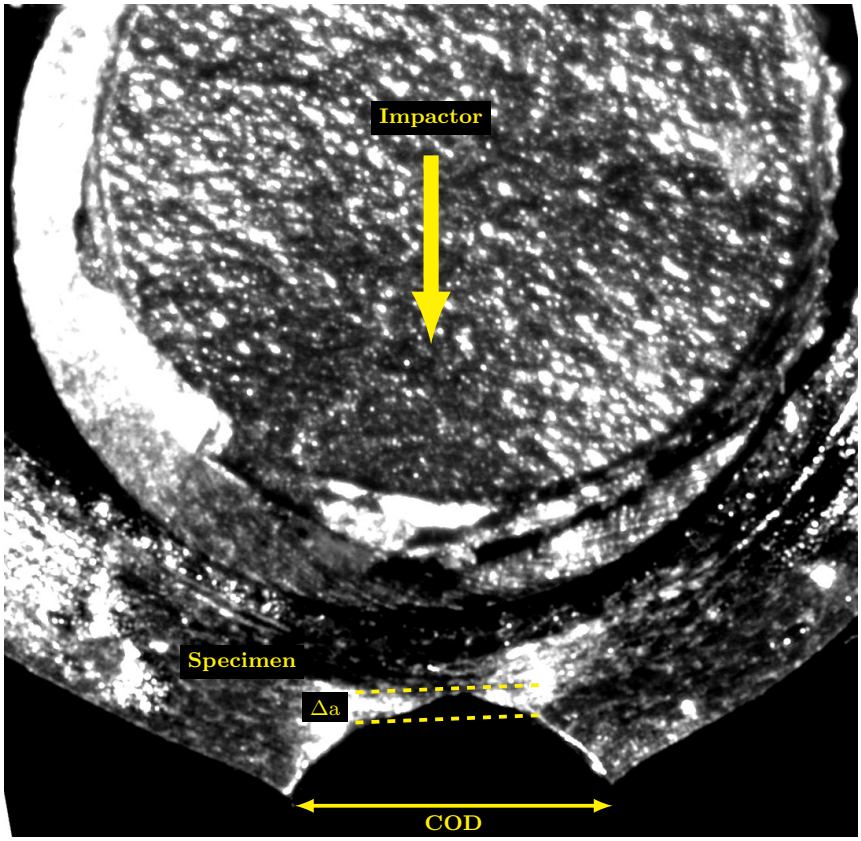

Fig. 7 Details of the blunted crack tip during the deformation; measurements of the Crack Opening Displacement (COD) and the crack extension (Δa).

at the same loading conditions. Only three of them were selected here to be presented since their reliability was considered as correct.

4.1.1 Crack Opening Displacement (COD)

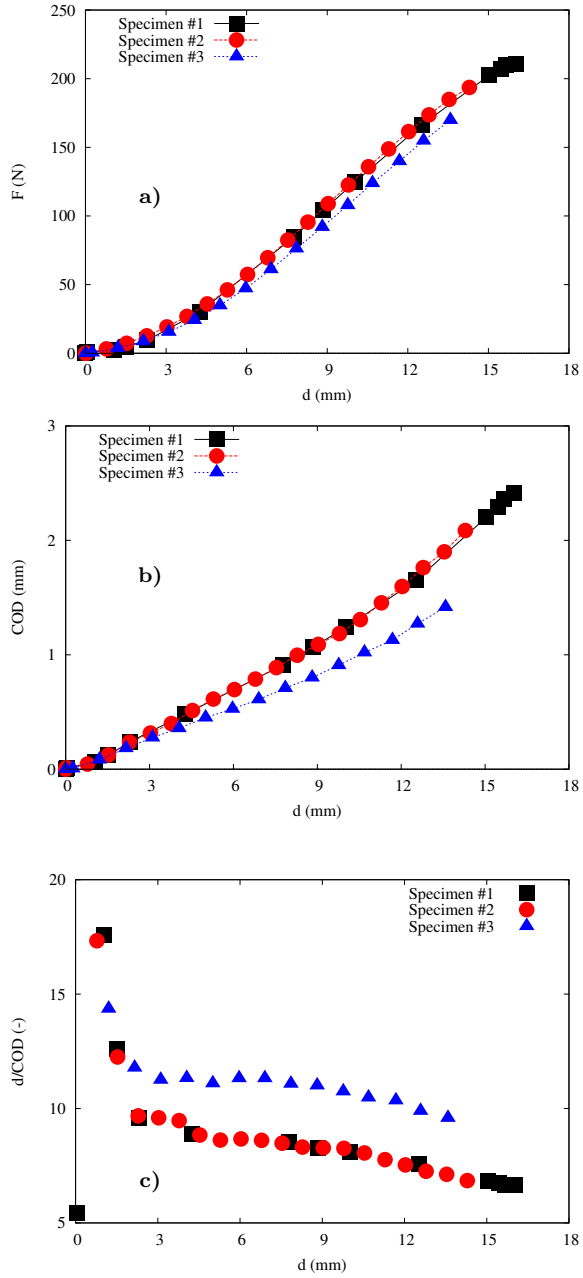

Fig. 8 Experimental data obtained from quasi-static test on clamped SENB specimen at room temperature: a) Load *vs.* deflection; b) crack opening displacement COD *vs.* deflection; c) the evolution of the ratio between the deflection and the COD.

The aim of fig. 8 was the analysis of the implication of the Crack Opening Displacement (COD) measurements to the classical load *vs.* deflection curve (fig. 8a). The experimental data were obtained from the three clamped SENB specimens with respect to the deflection. In fig. 8a, the initial inflexion was due to the gradual compression applied to the scored thin plate. A small linear part was observed after this inflexion, followed by a slight non linearity when approaching the maximum load. This latter point corresponded to the critical load at failure.

Figure 8b plots the COD as a function of the deflection. By contrast to what was reported with the usual SENB geometry [19], non-linearities could be noticed in the relationship between the deflection and the COD. To go further, the evolution of the ratio of the deflection by the COD was plotted in fig. 8c. A transient stage could be observed up to a deflection of 3 mm. This could be attributed to the gradual compression of the specimen in the beginning of the test. Then, between 3 mm and 8 mm approximately, this ratio exhibited either a stabilization at 11.5 for Specimen #3, or a very small decreasing rate for Specimen #1 and Specimen #2. These latters showed a good reproducibility and the average value of the ratio was estimated to be 8.

In the last part of the loading (from a deflection of 8 mm up to the failure), a continuous decrease of this ratio was observed, clearly highlighting non linearity between the deflection and the COD.

The use of these macroscopic measurements together with the COD allowed the calculation of respectively Γ (see eq.(2)) and J_p/η_p (see eq.(4)). Recall that $A(F, d)$ in eq.(2) and $A_t(F, COD)$ in eq.(4) were numerically integrated over the loading: Γ and J_p/η_p depend on the loading step. Their critical values Γ_c and J_c/η_p have to be determined at the moment of the failure. It should be noted that for classical (*i.e.* non clampled) SENB specimen the COD is proportional to the deflection and the calibration factor is known. Therefore, the two load parameters, as well as their critical values differ by a fixed multiplier factor. The above mentioned non linearities motivated further analysis concerning the material and specimen geometry under study.

Figure 9a shows a continuous increase of Γ as a function of the deflection for the three specimens. While good agreement was obtained for Specimen #2 and Specimen #3, a large deviation was observed for Specimen #1.

An attempt was then made to plot J_p (see eq. (4)) with respect to the deflection. Since the calibration factor η_p was unknown, the study focused on the reduced load parameter $\dfrac{J_p}{\eta_p}$ in fig. 9b. The same conclusion as for Γ could be mentioned although the values were one order of magnitude lower.

Table 1 summarizes the values at failure of the characteristic parameters. A large scatter could be observed in Γ_c and $\dfrac{J_c}{\eta_p}$ in the two last columns. Furthermore, the scattered Γ_c values significantly differed from the impact strength in the ductile plateau given in fig. 3: (0.25 kJ/m^2 *i.e* factor 100). This is problematic from mechanical engineering viewpoint. Indeed, Γ_c value

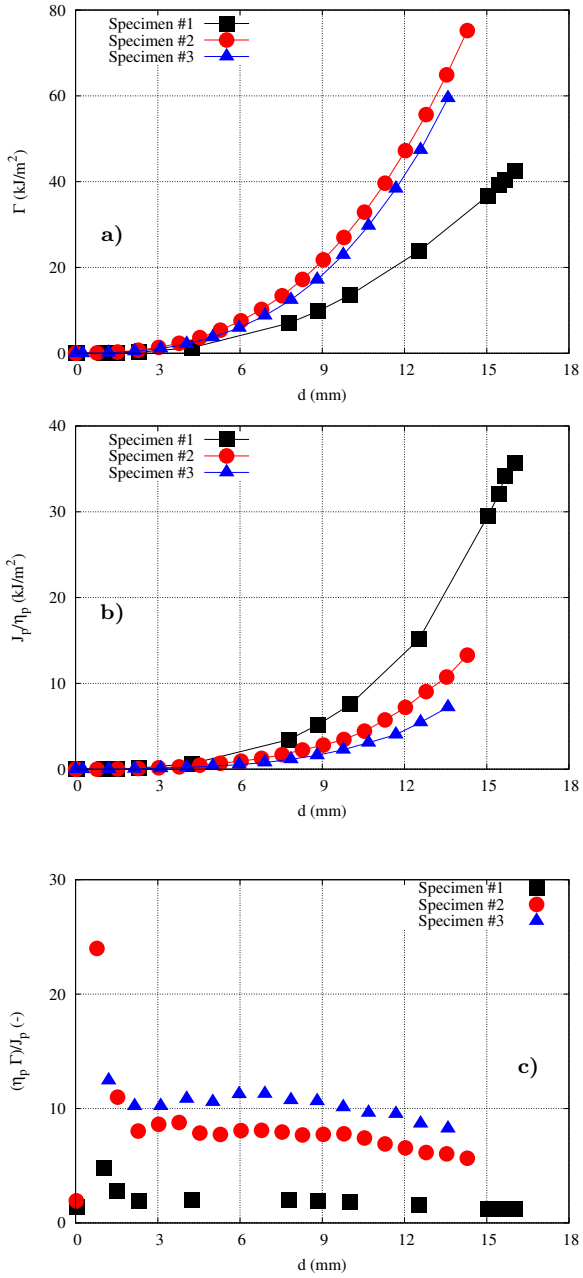

Fig. 9 Evolution as a function of the deflection of: a) The fracture energy related to the net cross section area; b) The J-integral related to η; c) The ratio between the two above mentioned parameters

Table 1 Values at failure of the collected experimental data (deflection, load and COD), followed by the fractured surface energy density Γ_c and fracture toughness $\frac{J_c}{\eta_p}$ calculated as the values at failure of respectively Γ and $\frac{J_p}{\eta_p}$.

Specimens	**d (mm)**	**F (N)**	**COD (mm)**	Γ_c **(kJ/m^2)**	$\frac{J_c}{\eta_p}$ **(kJ/m^2)**
#1	16.04	210.8	2.41	42.5	37.5
#2	14.29	193.6	2.09	75.2	13.3
#3	13.59	169.9	1.42	59.4	9.21

is required for the design and the safety of the airbag window during the deployment.

Further analysis was carried out by focusing on the ratio of Γ to $\frac{J_p}{\eta_p}$. In fact, from eqs. (2) and (4), this ratio could be expressed as follows:

$$\frac{\eta_p \Gamma}{J_p} = \frac{\eta_p d}{COD} \tag{5}$$

It can be seen that this ratio is a function of the unknown calibration factor η_p and the ratio of the deflection to the COD already plotted in fig. 8c. Figure 9c shows the evolution of the ratio $\frac{\eta_p \Gamma}{J_p}$ as a function of the deflection. As expected, the curve followed the same trends as that of $\frac{d}{COD}$ in fig. 8c. It should however be mentioned that the calibration factor η_p is dependent on the crack depth ratio a/W. Therefore, for a **stationary** crack, its constant value can be deduced, allowing the determination of both J_p and the multiplication factor between the impact strength and the fracture toughness.

By applying this methodology for the data in Table 1, *i.e.* for the values at failure, η_p was estimated to be 0.17, 0.83 and 0.67 respectively for Specimens #1, #2 and #3. This large scatter cannot be used as such in a mechanical engineering calculation for design and safety. Further investigation was carried out and developed in the following.

4.1.2 Crack extension Δa

For the three specimens, the evolution of the crack extension during the test was plotted with respect to the deflection in fig. 10a. A key point arose from the curves altogether: the crack systematically initiated very early, at a deflection of about 8 mm, corresponding to a load of about 80 N; that is, less than half of the load at failure mentioned above. After this initiation, the crack progressed

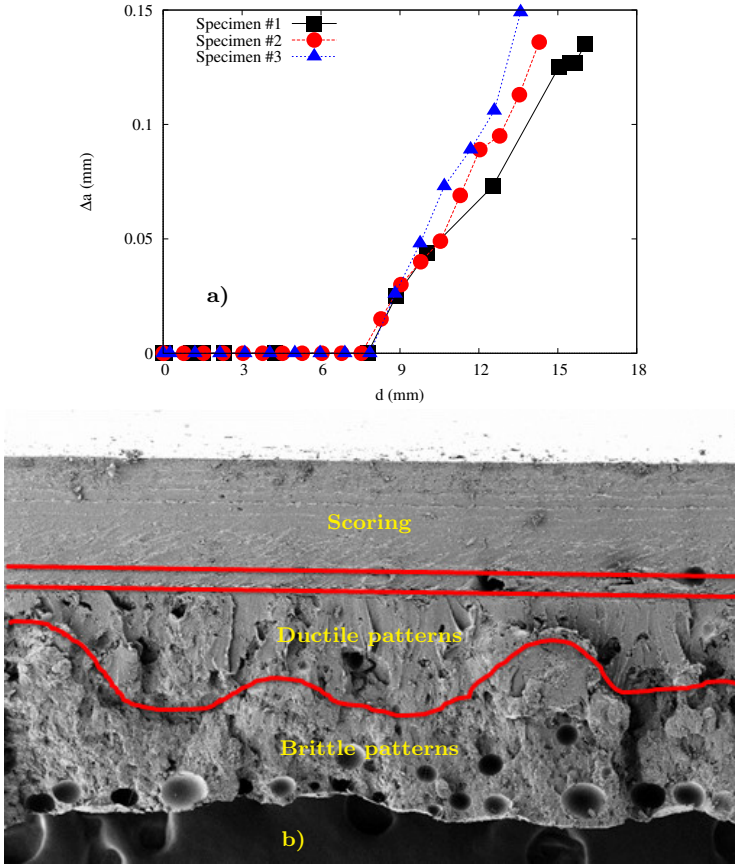

Fig. 10 Information about the cracking: a) Evolution of the crack extension Δa with respect to the deflection; b) Representative SEM examination of the fracture surface.

quasi-linearly as the deflection increased. The maximum crack extension measured at the lateral surface, just before the failure of the specimen, was about 0.15 mm. Figure 10a clearly evidenced that the crack was not stationary: the depth ratio a/W evolved from 0.5 to 0.625 when the deflection ran from 8 mm to about 15 mm.

Fracture surface examinations were carried out by Scanning Electron Microscopy so as to analyse the through thickness crack extension. Figure 10b illustrates the main features observed on a representative fracture surface after the tests (with permanent set). The initial crack implanted by the robot (scoring) exhibited a specific fracture surface with somes apparent striations due to the marks of the blade of the robot. Ahead of this pre-existing crack, an area surrounded by the two red straight lines showed some deformed fibrils that could be attributed to the blunting of the initial crack. This pattern was then followed by a rather flat surface with non-regular crack extension. This

Table 2 Key experimental data at the crack initiation and at the failure of the specimens.

Specimens	**Δa (mm)**		**d (mm)**		**F (N)**		**COD (mm)**	
Events	**init.**	**fail.**	**init.**	**fail.**	**init.**	**fail.**	**init.**	**fail.**
#1	0	0.14	7.77	16.04	84.9	210.8	0.91	2.41
#2	0	0.14	7.53	14.29	82.4	193.6	0.89	2.09
#3	0	0.15	7.86	13.59	76.3	169.9	0.71	1.42

was considered as a ductile crack surface where the ductile crack propagation occured. One can refer to fig. 7 to observe the side views of the blunting and the ductile crack extension. Beyond this latter, a more rugged surface, assumed to be a brittle pattern, appeared up to the end of the thickness. The deduced scenario could be summarized as follows, consecutively to increasing deflection:

- Blunting of the crack tip;
- Ductile crack initiation;
- Stable crack growth (ductile tearing);
- Rapid crack growth: this ultimate "brittle" failure did not have the same characteristics as that obtained at very low temperature. Indeed, this happened after the ductile tearing, thus, at a larger crack depth ratio and no fragmentation of the sample was observed.

The observed surface was not exactly at mid-thickness so that the average depth might be larger elsewhere. Several bubbles (voids/cavities), with an average diameter of about 0.05 mm, were observed on the fracture surfaces. Although their effects were not in the scope of this paper, it can be expected that their presence affected the reproducibility of the experimental data.

It can be deduced from these observations that the maximum load and the crack initiation did not coincide. The key experimental data at both crack initiation and the failure of the specimen were gathered in Table 2.

When using the fracture mechanics concepts, the curve to be analysed should be the load *vs.* the crack opening displacement (COD). Following Hale and Ramsteiner [6], a linear correction had to be operated so as to prevent the effects of the non-linearity due to penetration of the loading pins into the sample. To this end, the stiffness – defined as the inverse of the compliance of the specimen – was calculated as the derivative, point by point, of the load with respect to the COD: dF/d(COD). The evolutions of this stiffness as a function of the applied deflection were plotted in figs. 11a-c, superimposed with the evolution of the crack extension, corresponding to the second Y-axis. Two significant conclusions could be deduced from these curves:

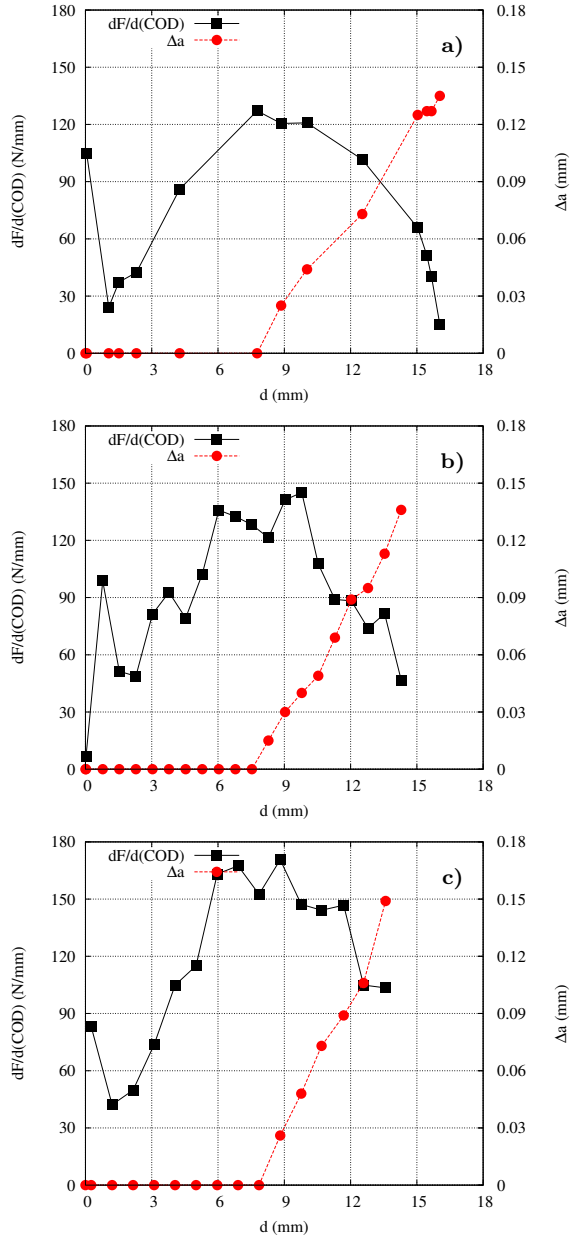

Fig. 11 Decrease of the stiffness correlated to the increase of crack extension for: a) Specimen #1; b) Specimen #2; c) Specimen #3.

– In contrast to the classical SENB data, the linear correction affected a larger part of the load *vs.* COD curve. There was no plateau of the stiffness corresponding to the elastic compliance of the curve;

– The stiffness decreased as soon as the crack extension started to progress; meaning that the non linearity in the load *vs.* COD curve was essentially due to the crack initiation and growth, but not to the plasticity.

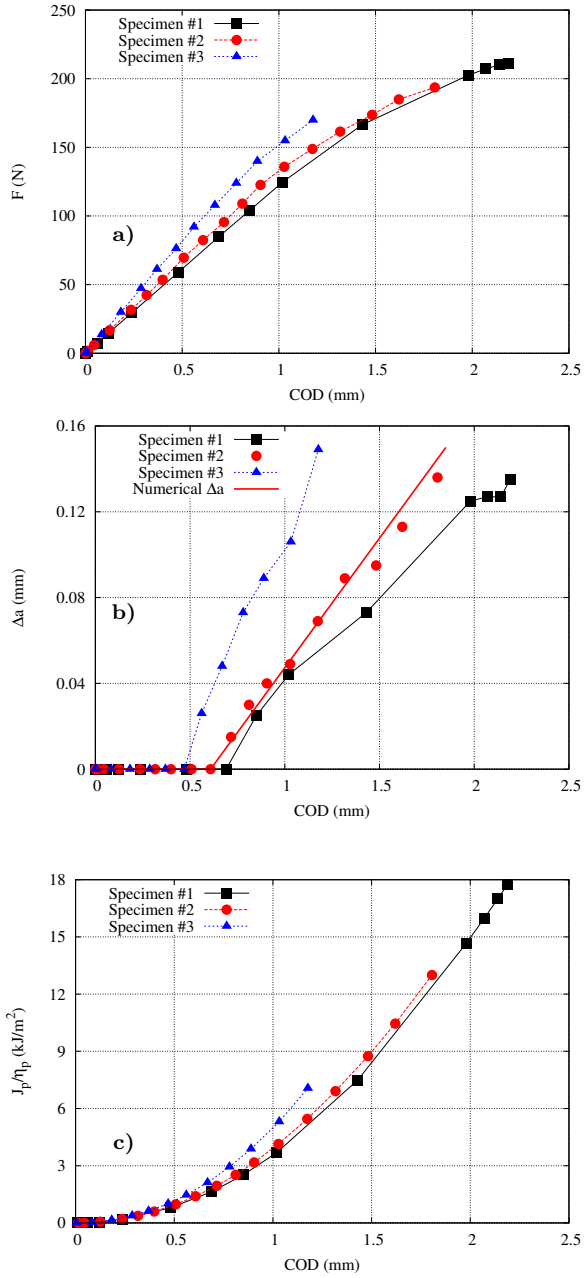

Fig. 12 Evolution as a function of the COD of: a) The load "F"; b) The crack extension Δa; c) The J-integral related to η_p.

In order to prepare for fracture mechanics concepts to be applied, namely using finite elements (FE) analysis, the same key curves as in figs. 8-9 were plotted, once the linear correction has been applied, as a function of the COD in fig. 12.

Figure 12a displays the load *vs.* COD curves showing the corrected linear part. The stiffness was estimated to be 140 ±20 N/mm. The last experimental points corresponding to the failure of the specimens, a large scatter could be observed concerning the COD at failure. Especially, the curve of Specimen #3 had a small COD at failure in comparison with the two others.

As mentioned above, the trend of the crack extension as a function of the COD in fig. 12b showed stable growth of about 0.15mm before the abrupt failure: the crack depth ratio a/W evolved from 0.5 to 0.625. Again, Specimen #3 showed a steeper slope meaning a more brittle failure. The solid red line in fig. 12b illustrates a fit of the crack extension of Specimen #2. This was used as boundary condition for the FE release nodal degree of freedom technique.

The knowledge of the crack extension allowed the calculations of J_p/η_p (eq. (4)) by updating the actual crack depth. In fig. 12c, after correction of the linear part, J_p/η_p was plotted as a function of the COD. These curves showed less scatter and smaller values of J_p/η_p than in fig. 9b.

Table 3 Load parameter $\frac{J_p}{\eta_p}$ calculated from experimental data after linear correction of the COD.

Specimens	**Δa (mm)**		**COD(mm)**		**F(N)**		$\frac{J_p}{\eta_p}$**(kJ/m²)**	
Events	**init.**	**fail.**	**init.**	**fail.**	**init.**	**fail.**	**init.**	**fail.**
#1	0	0.14	0.69	2.19	84.9	210.8	1.64	17.8
#2	0	0.14	0.61	1.81	82.4	193.6	1.40	13.0
#3	0	0.15	0.47	1.18	76.3	169.9	1.01	7.06

Table 3 displays the characteristic values of the main mechanical parameters obtained experimentally followed by the corresponding J_p/η_p. Apart from Specimen #3, J_p/η_p at crack initiation was 10 times less than at failure.

Specimen #2 data set was selected for the FE simulation of propagating crack. Indeed, specimen #3 was mentioned to exhibit some deviation compared with the two others; whereas Specimen #1 showed a peculiar crack growth behaviour at the onset of the failure (see black full square in fig. 12b).

4.2 FE simulations

The purpose of the FE simulations was essentially to numerically compute the J-integral load parameter so as to compare it with that of eq. (4). J-integral being dependent on the crack depth, three specific conditions were simulated:

- A stationary crack with the initial crack depth a_0;
- A stationary crack with the ultimate crack depth a_f;
- A propagating crack from a_0 to a_f.

Furthermore, the release nodal degree of freedom (`rndof`) technique was assigned to follow the fit of the crack extension (red solid line) in fig. 12b.

4.2.1 Inverse optimization of the material parameters

Before computing the J-integral load parameter, the material parameters were determined by using inverse method of optimization in the Zset suite. This optimization was performed using the load *vs.* COD with the propagating crack. Therefore, the simulated curve –to be compared with the experimental one– accounted for the crack growth using the `rndof` technique. A simple elasto-plastic model was used during the optimization.

Figure 13a illustrates the comparison of the experimental (full circles) with the simulated (solid line) load *vs.* COD curves, obtained from the optimized material parameters. The oscillations observed in the simulation response were due to the discrete crack growth applied on the three isoparametric elements ahead of the crack tip.

Figures 13b-c show the opening stress contour map on the deformed specimen (left) and the deformed crack tip (right), respectively at the onset of crack initiation (crack depth = a_0) and at the onset of the brittle failure, that is, at the end of the ductile crack propagation leading to a crack depth of a_f.

Note that the remaining ligament (W-a_0) is longer in fig. 13b than in fig. 13c, with (W-a_f). This indicated that the numerical crack growth was actually operated. Furthermore, the impactor was observed to detach from the top of the PVC specimen at these loading steps. This phenomenon was also experimentally observed –even though not very clear– in fig. 7.

Once the material parameters obtained, two simulations with stationary cracks (a_0 and a_f) were carried out so as to compare the compliance of the system (see fig. 13a):

- Red full square symbols correspond to the crack depth a_0. Obviously, the load *vs.* COD was in line with that of the propagating crack. Moreover, this curve was linear, meaning that linear fracture mechanics concept should be valid before the crack initiation;
- Blue full triangles represented the crack depth a_f. The compliance was clearly larger (lower stiffness) due to larger crack depth. The end of the load *vs.* COD showed a slight hardening, that probably was due to the contact configuration in figs.13b-c. However, the last point coincided with the propagating crack simulation.

4.2.2 Fracture toughness - Elastic calibration factor

Zset finite element code is provided with a routine allowing numerical J-integral to be computed using the de Lorenzi method [18]. For common fracture mechanics specimens such as SENB or CT, the numerical J-integral is correlated with J_p if the experiment and numerical load *vs.* COD curves are in good agreement, as this is the case in fig. 13a. Therefore FE J-integral, noted as J_{FE}, was assumed to be reliable for the clamped SENB specimen.

Seven J_{FE} were requested to Zset FE code according to the crack progress: at the initial crack depth (a_0), then at each crack extension of 25 μm until the final crack depth prior to failure (a_f). The stabilization of J_{FE} was checked thanks to 8 rows of elements surrounding each of the seven crack tips. Typically, it was obtained from the second or the third row of elements. Of course, if the crack tip did not correspond to that of the `rndof` procedure, the computed J_{FE} at this location was ignored.

In fig. 14, the seven values of J_{FE} were plotted with respect to the COD as black full square symbols. The blue full circle symbols were attributed to the "experimental" J_p/η_p.

Fracture toughness J_c

The determination of the fracture toughness requires the load *vs.* COD curve so as to calculate J-value and the corresponding crack extension Δa. As pointed out by Baldi *et al.* [9], a clear transition from the crack blunting phase to the fracture propagation is not easy to observe, especially for 3D crack shape in opaque polymers. It is often proposed to take, either the J-value at the maximum load or the J-value at a given amount of crack extension (0.2 mm for instance). In the present work, the fracture toughness J_c was assumed to be the value of J_{FE} at the crack initiation. From fig. 14, it was estimated to be 10.8 kJ/m^2. This value is very close to that obtained by Hale and Ramsteiner [6] for a modified PVC: $J_{0.2}$=10.2 kJ/m^2.

Once the fracture toughness obtained, the evaluation of the calibration factor was attempted by using the value of J_p/η_p=1.4 kJ/m^2 at crack initiation for Specimen #2 in Table 3. The calculation allowed an estimate of $\eta_p \approx 8$ for the clamped SENB with a/W = 0.5, at least for the plasticized PVC under study. It should be mentioned that:

- This value is 4 times higher than that of classical (non clamped) SENB specimen;
- By considering eq. (3) and fig. 13a, where the load *vs.* COD was mentioned to be linear up to the crack initiation, it could be assumed that the obtained calibration factor was actually the elastic one η_e. Indeed, at this stage, $A_p(F, COD) = 0$ and $A_e(F, COD)$ corresponds to the area of the triangle (0, F, COD) at the crack initiation;
- The fracture toughness $J_c = 10.8$ kJ/m^2 should be used for the prediction of the crack initiation on engineering structures. Especially, on CEAST scored specimens tests [2], on the one hand, and on the window of the airbag box

located in the dashboard, on the other hand. As soon as the J-integral can be computed or calculated, the prediction consists of a comparison between the value of J-integral with J_c.

4.2.3 Crack propagation

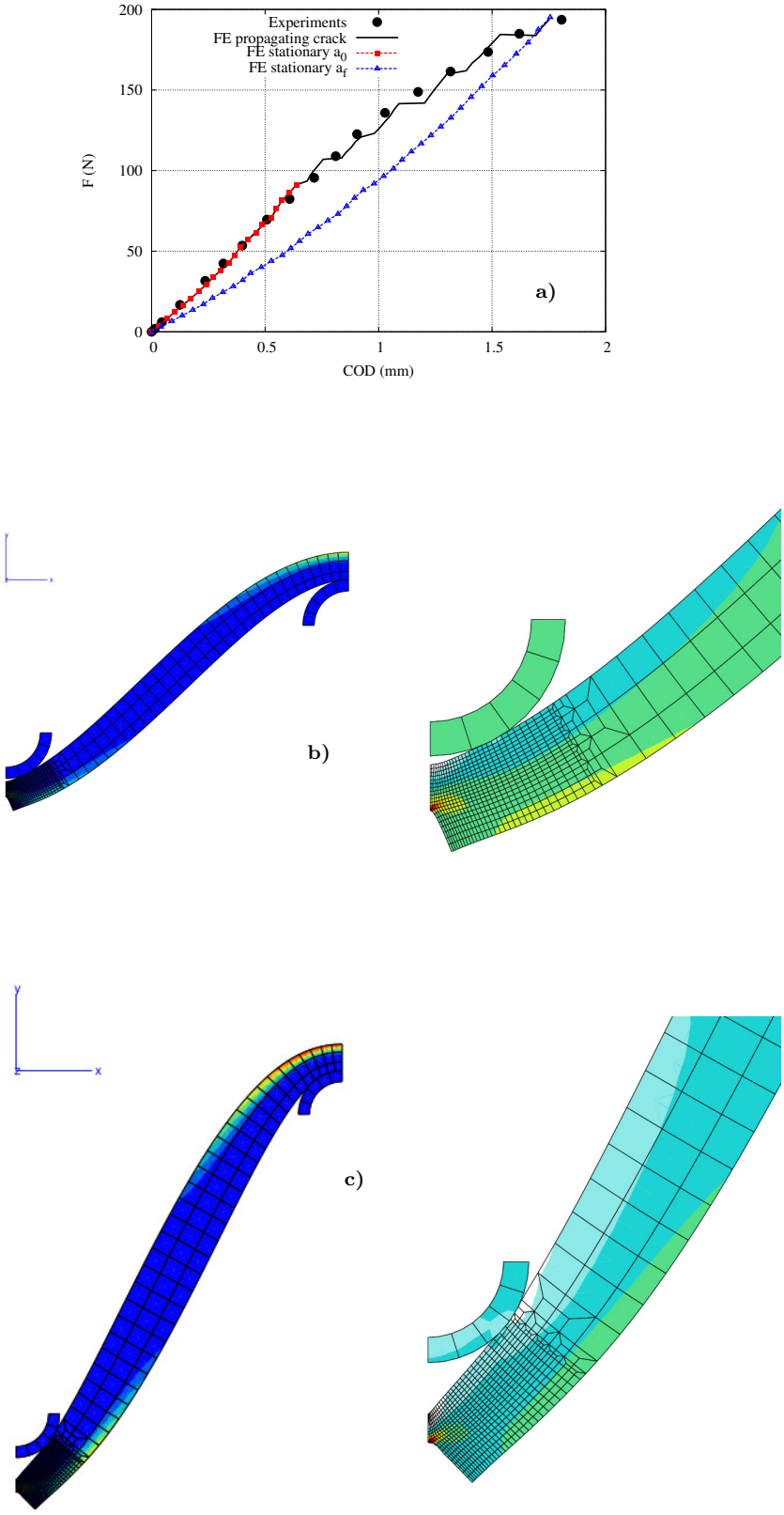

Fig. 13 a) The load *vs.* COD curves for various configurations; Opening stress contour map on the deformed crack tip: b) at the end of the linear part; c) at the end of the ducile crack growth.

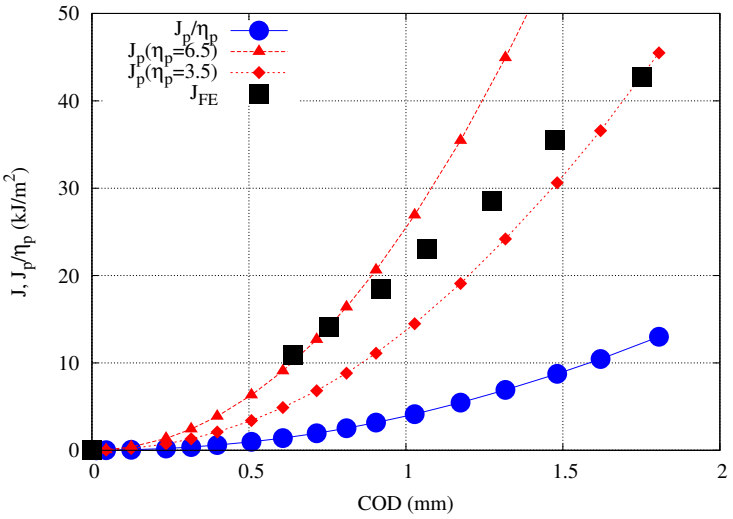

Fig. 14 The J-integral related to η_{p} as a function of the COD

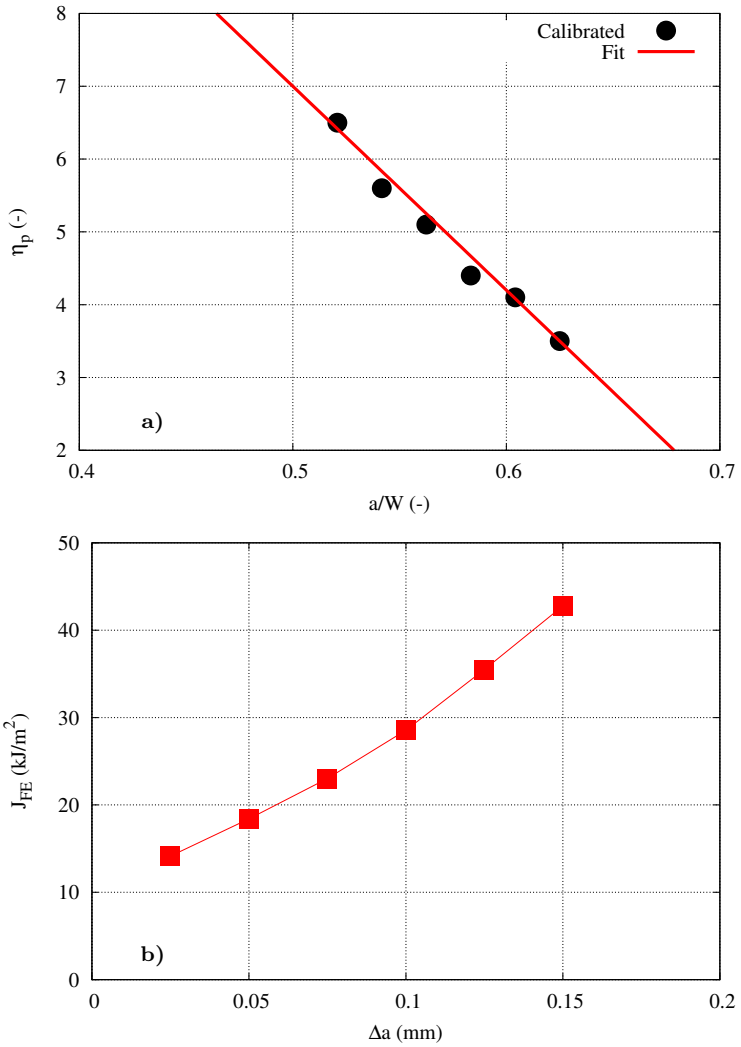

Fig. 15 The calibration factor η_p as a function of the crack depth ratio a/W.

Once the crack had initiated, the next experimental points dealt with crack growth ($\Delta a \neq 0$). The load *vs.* COD curve exhibited non linearity. In strict logic, this implies to separate the two calibration factors η_e and η_p in eq. (3), themselves depending on the crack depth ratio. To overcome this difficulty, the use of eq. (4) was proposed here. The evolution of η_p as a function of a/W was determined by using the total area under the load *vs.* COD curve. To this end, a multiplicative factor was attributed to each of the six remaining J_{FE} in fig. 13a, so as for the "experimental" J_p/η_p curve to intersect this point. The red curves with triangle and diamond symbols in fig. 14 examplified this approach for, respectively, the second and the last J_{FE} values. These multiplicative factors were plotted as a function of the crack depth ratio in fig. 15a. A linear evolution of the η_p calibration factor could then be established, allowing an access to J-integral by using eq. (4) whatever the crack depth ratio.

Taking advantage of J_{FE} associated with Δa, an attempt was made to establish the crack growth resistance (R) curve of the studied plasticized PVC. The testing protocol for conducting J-crack growth resistance curve tests on plastics consists of using multiple specimens with various crack depths [6]. Recent works carried out under the direction of the Technical Committee 4,"Polymers, Polymer Composites and Adhesives," of the European Structural Integrity Society (ESIS TC4) suggested the use of two specimens so as to obtain the R-curve [10,11]. The following results represent a contribution to this active work on fracture of plastics.

Figure 15b displays J-Δa from Specimen #2 data assisted by FE analysis. The six points allow the prediction of the ductile crack growth in this material on a small amount of crack extension. However, when attempting to plot the blunting line, it was far below this J-Δa curve. This blunting assumed to be semi-circular [5] theoretically can be estimated to be half of the crack tip opening displacement. As mentioned above, fig. 7 showed a large blunting of the crack tip. This result could have been expected. Further assessment should be carried out before using safely the present J-Δa curve.

5 Discussion

This section focuses on the methodology allowing the transferability [20] of the clamped specimen results, in terms of crack initiation and propagation, into the CEAST tests first and by extension to the dashboard. A major assumption should be outlined here: the temperature and the impact speed selected locate the test in the upper shelf of the fracture toughness curve. The ductile mechanisms operate and J_c=10.8 kJ/m^2 and the R-curve are considered to be valid.

5.1 From clamped SENB to CEAST test results

Recall that the geometries of the impactors were circular (round bar) and hemispherical for the clamped SENB and the CEAST tests, respectively. The

mechanisms of crack initiation and growth differed in the portion of process zone in the remaining ligament. Whereas for clamped SENB the whole width (29.8 mm) was involved, in the CEAST specimen the sequence was as follows:

- when the impactor tip entered in contact with the top surface of the sample at the end of the remaining ligament, only a small portion of the diameter (Φ) of the impactor was concerned with the crack initiation;
- this initiated crack propagated through the thickness;
- the displacement of the hemispherical impactor induced lateral crack propagation, *i.e.* perpendicular to the direction of the impactor displacement.

The approach should be based on the crack initiation, *i.e.* as soon as J_c=10.8 kJ/m^2 is reached. For CEAST tests, only the load *vs.* deflection was available. For mechanical engineering purpose, namely the safety engineering design of structures, the salient question is how to determine the ductile crack initiation from these data.

By using a FE code, the approach consists of computing the J-integral value on the meshed CEAST specimen using an elastic-visco-plastic model. The experimental load *vs.* deflection curve should be in agreement with the simulated one at each test temperature and impact speed. When the J-integral reaches the fracture toughness value 10.8 kJ/m^2, the crack initiation is supposed to be established and the computation should be stopped.

The analytical approach is more complex. Recall that at the crack initiation for clamped SENB specimens, the load *vs.* COD curve was linear so that, on the one hand, the calibration factor is equal to the elastic one ($\eta_e \approx 8$); on the other hand, fig. 8c indicated that the deflection of about 8 mm is proportionnal to the COD.

Since the crack initiation was detected at the COD where the stiffness (inverse of the compliance) decreased, it should be also valid for the stiffness in terms of load *vs.* deflection curve. This operation was carried out directly on the data of the CEAST tests in fig. 2. For the three tests, the stiffness increased first up to a deflection of 8 mm, then stabilized between 8 mm and 10 mm to decrease at last. The crack initiation was assumed to occur at 10 mm for CEAST tests at 23°C and 4.4 m/s. To go further, the energy A(d = 10mm) according to eq. (1) is equal to 2 $\pm$ 0.1 J. This energy should be related to the fractured surface used to the determination of the impact strength ($\Phi(W - a_0)$), giving 0.11 kJ/m^2. This value is twice lower than the upper shelf impact strength in fig. 3 (0.25 kJ/m^2). But, it corresponds to the actual crack initiation, in agreement with the fracture toughness of the material. This "impact strength at crack initiation" should be assessed by using all the CEAST experimental data:

- by determining the deflection from which the stiffness decreases;
- by integrating the area under the load *vs.* deflection curve up to the selected deflection, so as to estimate the energy at crack initiation;
- by relating this energy to the area of the remaining ligament assumed to be $\Phi(W - a_0)$

Using this consolidated value should be recommended regarding the significant result of the present work.

5.2 From CEAST results to the full scale test on dashboard

For a real engineering structure like the dashboard, only FE analysis would be efficient for the prediction of the crack initiation to allow the correct deployment of the air bag. To this end, the window of the air bag box (fig. 1) should be meshed in detail. The three layers of materials as well as the scoring in the PVC skin should be discretized with sufficiently refined meshes. The challenge is to reduce the numerical cost of such a study.

The same material parameters of elasto-visco-plastic model that have been identified for the CEAST tests at the temperatures and impact speeds located in the upper part of the diagram of fig. 4 should be used.

The boundary conditions should be associated to the kinetic energy due to the air bag deployment. The safe opening of the window, in ductile mechanisms, corresponds to the precise conditions (time, temperature, loading...) allowing the J-integral to attain the fracture toughness of the material.

Once this goal achieved, many parameters of interest can be optimised to ensure a safe deployment of the air bag:

- the formulation and the processing of the material to obtain an efficient time and temperature dependent constitutive model;
- the drawing of the scoring as straight line, Y or U or L shaped that already exist;
- the score depth ratio: it was shown that for 0.625 a net brittle failure, without branching or fragmentation of the skin, occurred;
- the kinetic energy due to the air bag display.

6 Concluding remarks

The desired fracture process allowing the safety of the passengers during the deployment of the airbag in automative industry is the ductile failure. Full scale experiments on dashboard showed that the impact speed was estimated to be 25 m/s and at 23 °C, a ductile failure of the skin –made of plasticized PVC– was evidenced. This result was in agreement with the domain of temperatures and impact speeds established with drop tower tests at lower speeds/temperatures [2].

Dedicated clamped SENB specimens were used to characterize the mechanisms of ductile crack initiation and propagation for the studied material. In contrast to the route recommended by non linear fracture mechanics, the crack initiation occured before the maximum load prior to the final failure of the specimen. In fact, it was observed when the loss of linearity in the load *vs.* COD appeared. Thanks to the "release nodal degree of freedom" procedure,

the in-house FE code allowed the simulation of the crack extension to be performed. The calibration factor of the clamped SENB specimen with respect to the crack depth ratio was established. Moreover, the fracture toughness J_c, defined as the numerical J-integral at the crack initiation, was evaluated to be 10.8 kJ/m^2, in agreement with values reported in the literature.

Focusing on the crack initiation, the corresponding impact strength for the previous drop tower tests in the upper shelf was corrected. Instead of the previous 0.25 kJ/m^2 this critical value was reduced to 0.11 kJ/m^2. The modified fracture toughness and the impact strength values were proposed in the methodology allowing the ductile crack initiation to be predicted:

- for the drop tower test results where the COD and the crack extension were not available. Two methods were proposed.
  - by running FE analysis of the test and selecting the time when the J-integral reached the value of 10.8 kJ/m^2;
  - by detecting the loss of linearity in the load *vs.* deflection curve for which the fractured surface energy density was equal to 0.11 kJ/m^2
- for the dashboard where the plasticized PVC skin was integrated. Once the whole structure was meshed, FE simulation of the airbag display should be performed up to the time when the numerical J-integral reached the value of 10.8 kJ/m^2

It was mentioned that using FE code would allow the optimization of many parameters to lead to a safe deployment of the air bag.

Acknowledgements The authors would like to acknowledge Gabriel Dalloux and Grégory Martin (Nakan Company) for their fruitful discussions. Jean Christophe Teissedre is acknowledged for technical assistance.

References

1. K.R. Cox and R.E. Robertson, Controlling Failure of Polymer Skin/Foam Bilaminate Sheets, SAE Technical Paper 2007-01-1216, SAE International, Warrendale, PA, (2007)
2. C. Bertaux, N. Amouroux, C. Ovalle Rodas, L. Laiarinandrasana, Impact speed dependency of the ductile failure threshold temperature for a plasticized Polyvinylchloride, *submitted to* Continuum Mechanics and Thermodynamics (2020)
3. ISO 179-1:2010, Plastics – Determination of Charpy impact properties – Part 1: Non-instrumented impact test. https://www.iso.org/
4. ASTM D6110, Standard Test Method for Determining the Charpy Impact Resistance of Notched Specimens of Plastics https://www.astm.org/Standards/D6110
5. J.G. Williams, K_C and G_C at low speed for polymers, Fracture Mechanics testing methods for polymers, adhesives and composites, Edited by D.R. Moore, A. Pavan and J.G. Williams, ESIS Publication 28 , p. 159-175, (2001)
6. G. Hale et F. Ramsteiner, J-Fracture toughness of polymers at slow speed, Mechanics testing methods for polymers, adhesives and composites, Edited by D.R. Moore, A. Pavan and J.G. Williams, ESIS Publication 28 p. 123–157 (2001).
7. ISO 6603-2:2000, Plastics – Determination of puncture impact behaviour of rigid plastics – Part 2: Instrumented impact testing. https://www.iso.org/en/standard/25172.html
8. B. Tanguy, C. Bouchet, S. Bugat, J. Besson, Local approach to fracture based prediction of the ΔT 56J and $\Delta TK_{Ic}100$ shifts due to irradiation for an A508 pressure vessel steel, Engineering Fracture Mechanics, 73, 191–206 (2006)
9. F. Baldi, S. Agnelli, T. Riccò, On the determination of the point of fracture initiation by the load separation criterion in J-testing of ductile polymers, Polymer Testing 32, 1326–1333 (2013).
10. S. Agnelli, F. Baldi, B.R.K. Blackman, L. Castellani, P.M. Frontini d, L. Laiarinandrasana, A. Pegoretti, M. Rink, A. Salazar, H.A. Visser, Application of the load separation criterion in J-testing of ductile polymers: A round-robin testing exercise, Polymer Testing 44, 72–81 (2015).
11. F. Baldi, S. Agnelli, L. Andena, B. Blackman, L. Castellani, P. Frontini, J. Kucera, L. Laiarinandrasana, A. Pegoretti, A. Salazar, L. Warnet, Determination of the Fracture Resistance of Ductile Polymers: The ESIS TC4 Recent Experience, Materials Performance and Characterization 9 (5), 675–687 (2020).
12. W. Bohme, H.J. MacGillivray, Experience with instrumented Charpy tests obtained by a DVM round-robin and further development, Evaluating Material Properties by Dynamic Testing ESIS 20, Edited by E. van Walle, Mechanical Engineering Publications, London p. 1-23, (1996)
13. L. Laiarinandrasana, Y. Nziakou, J.L. Halary, Fracture behavior of amorphous and semicrystalline blends of poly(vinylidene fluoride) and poly(methyl methacrylate), Journal of Polymer Science Part B: Polymer Physics, 50(24), 1740–1747 (2012)
14. J.H.Bulloch, A study concerning material fracture toughness and some small punch test data for low alloy steels, Engineering Failure Analysis, 11(4), 635–653 (2004)
15. H.J. MacGillivray, Fracture toughness of polymers at impact speed, Fracture Mechanics testing methods for polymers, adhesives and composites, Edited by D.R. Moore, A. Pavan and J.G. Williams, ESIS Publication 28 , p. 159-175, (2001)
16. L. Laiarinandrasana, M.R. Kabiri, M. Reytier, Effect of specimen geometries on the C* versus da/dt master curve for type 316L stainless steel, Engineering Fracture Mechanics 73, 726–737 (2006).
17. A. Marcellan, A. Bunsell, R. Piques, L. Laiarinandrasana, In Situ Tensile Tests to Analyze the Mechanical Response, Crack Initiation, and Crack Propagation in Single Polyamide 66 Fibers, Journal of Polymer Science, Part B: Polymer Physics 57, 680–690 (2019).

18. H.G. de Lorenzi, On the energy release rate and the J-integral for 3-D crack configurations, International Journal of Fracture 19, 183 –193 (1982).
19. M. Challier, J. Besson, L. Laiarinandrasana, R. Piques, Damage and fracture of polyvinylidene fluoride (PVDF) at 20°C: experiments and modelling, Engineering Fracture Mechanics, 73, 79–90 (2006)
20. W.Brocks, G.Knecke, H.D. Noack, H.Veith, On the transferability of fracture mechanics parameters from specimens to structures using fem, Nuclear Engineering and Design, 112, 1–14 (1989).